Electronic Supplementary Material (ESI) for Green Chemistry

Facile route fabrication of nickel based mesoporous carbons with high catalytic performance towards 4-nitrophenol reduction

Ying Yang,[*a] Yang Ren,[b] Chenjun Sun[b] and Shijie Hao[a]

[a]State Key Laboratory of Heavy Oil Processing, China University of Petroleum, Changping, Beijing 102249, China

[b]X-ray Science Division, Argonne National Laboratory, 9700 S. Cass Ave., Argonne, Illinois 60439, USA

Contents:

Fig. S8 FT-IR spectra of (a) Ni/CTS-P, (b) Ni/MC-550, (c) Ni/MC-750 and (d) Ni/MC-950.

Fig. S9 H_2 chmisorption results for (A) Ni/MC-550, (B) Ni/MC-750 and (C) Ni/MC-950.

Fig. S10 TEM image of the spent Ni/MC-750.

1 Materials preparation

1.1 Preparation of 5-chloromethyl-8-quinolinol hydrochloride

A mixture of 5.84 g (70.0 mmol) of 8-quinolinol, 50 ml of concentrated hydrochloric acid, and 6.4 ml of 37% formaldehyde was treated with 0.6 g of zinc chloride and stirred overnight. The mixture was filtered, washed with copious acetone and dried to give the title compound 1^{C}·HCl as a yellow solid (7.02 g, 90%). Found: C, 52.44; H, 3.86; N, 5.84%. Calc. for $C_{10}H_8NOCl$·HCl: C, 52.17; H, 3.91; N, 6.08%. ^{1}H NMR (D_2O, TMS, δ ppm): 9.24 (1H, d, C(2)H), 8.96 (1H, m, C(4)H), 8.06 (1H, m, C(3)H), 7.68 (1H, s, C(6)H), 7.36 (1H, s, C(7)H), 5.03 (2H, s, CH_2Cl) (Fig. S1). UV-vis, λ (nm): 258, 313, 376 (Fig. S2). FTIR (KBr pellets, cm^{-1}): 3386 (Ph-OH), 1627, 1594 (C=C/C=N), 1550, 1452 (Ph), 1390 (C-N), 1087 (C-O), 819, 769 (C-H), 694 (C-Cl) (Fig. S3).

1.2 Preparation of 8-quinolinol modified chitosan

Chitosan (0.9 g) was mixed with 50 ml of 20 wt% HAc, and stirred for 1 h. Then 4.6 g of 1^{C}·HCl combined with 60 ml of 36 wt% Et_3N was added and stirred for further 36 h. The mixture was filtered, washed with ether, ethanol and deionized water, and dried to give light yellow solids, denoted as CHS-HQ. UV-vis, λ (nm): 243, 318, 429 (Fig. S4). FTIR (KBr pellets, cm^{-1}): 3063 (NH), 2921, 2863 (CH_2), 1623 (C=N), 1580, 1507, 1740, 1418, 1365 (Ph), 1265, 1228, 1197, 1155, 1113, 1070, 891, 828, 781, 703 (Fig. S5).

2 Characterization

UV-vis spectra were recorded on a Perkin Elmer spectrophotometer Lambda 650s using barium sulfate as the standard in the range 200-800 nm. The infrared spectra (IR) of samples were recorded in KBr disks using a NICOLET 6700 spectrometer.

Liquid ^{1}H spectra were recorded on a Varian Mercury-300 MHz instrument using tetramethylsilane (TMS) as the internal standard. Small-angle X-ray scattering measurements were performed at the 12-ID-C station at the Advanced Photon Source (Argonne National Laboratory, Argonne, IL). The X-ray energy was 12 keV, which corresponds to a wavelength of 1.0332 Å. The sample-to-detector distance was about 2 m. A 2D CCD detector was used to acquire images with typical exposure times in the range of 0.01-1 s. The EXAFS function, $\varkappa$, was obtained by subtracting the post-edge background from the overall absorption and then normalized with respect to the edge jump step. The normalized $\varkappa(E)$ was transformed from energy space to k space, where k is the photoelectron wave vector of x-rays. The $\varkappa(k)$ data were multiplied by k^2 to compensate the damping of EXAFS oscillations in the high k region. Subsequently, k^2-weighted $\varkappa(k)$ data in k space ranging from 3.6 to 12.6 $Å^{-1}$ for the Ni K-edge were Fourier transformed to r space to separate the EXAFS contributions from the different coordination shells. A nonlinear least-squares algorithm was applied to the curve fitting of an EXAFS in r space between 0.7 and 3.3 Å for Ni depending on the bond to be fitted. The effective scattering amplitude [f(k)] and phase shift [δ(k)] for Ni-Ni were generated by using the FEFF7 code. The reference phase and amplitude for the Ni-Ni absorber-scatter pairs were obtained from a Ni foil. All the computer programs were implemented in the UWXAFS3.0 package, with the backscattering amplitude and the phase shift for the specific atom pairs being theoretically calculated by using the FEFF7 code. From these analyses, structural parameters such as the coordination numbers (CN), bond distance (R) and Debye-Waller factor ($\Delta\sigma_j^2$) and the inner potential shift (ΔE_0) have been calculated. The fitting procedure resulted in estimated accuracy of ±20% for the first shell CN, ±1% for the bond distance and ±10% for the Debye-Waller factor.

Fig. S1 ^{1}H NMR spectrum of 1^{C}·HCl.

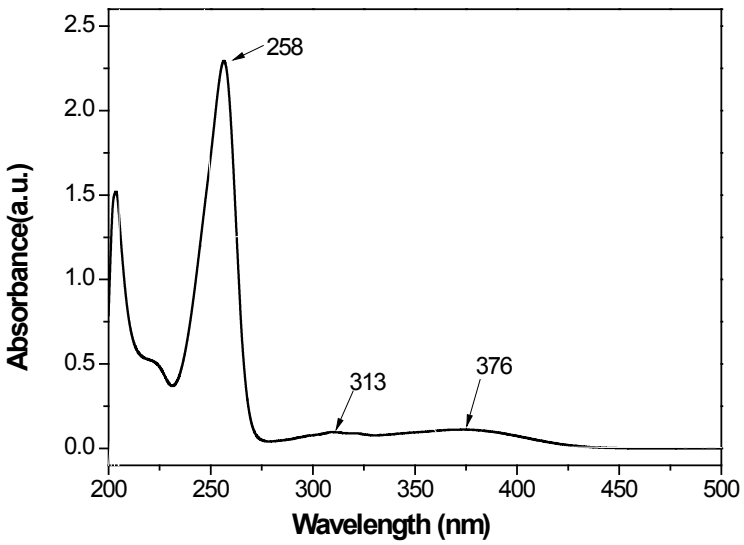

Fig. S2 UV-vis spectrum of 1^{C}·HCl.

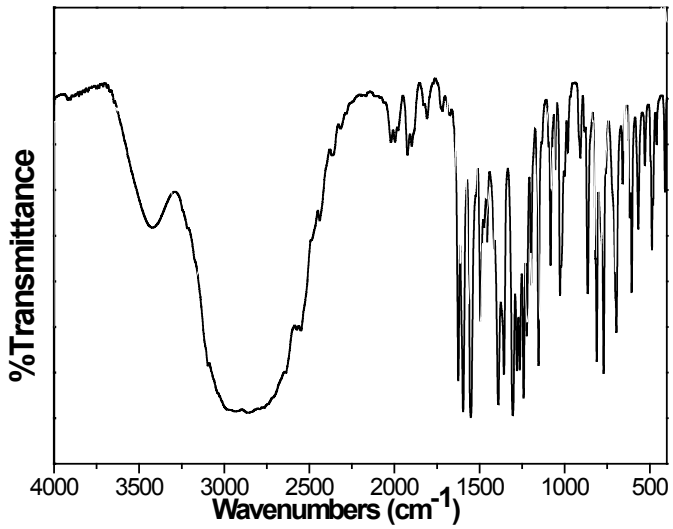

Fig. S3 FT-IR spectrum of 1^{C}·HCl.

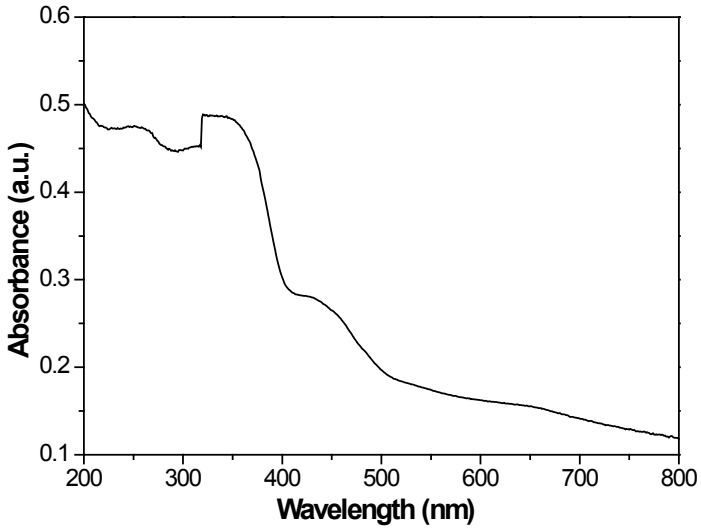

Fig. S4 UV-vis spectrum of CTS-HQ.

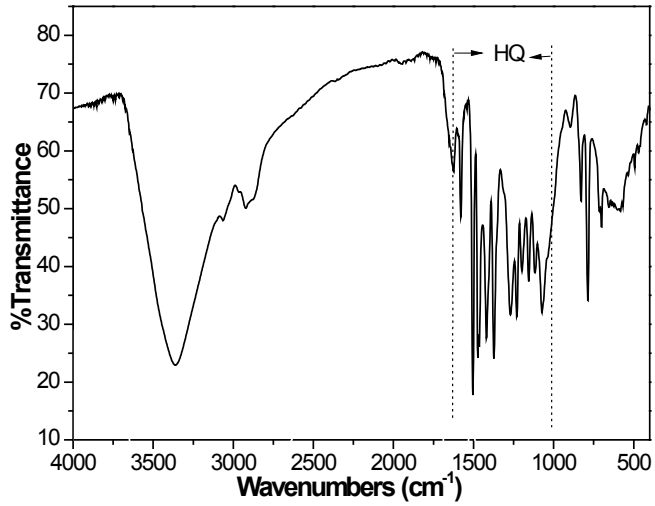

Fig. S5 FT-IR spectrum of CTS-HQ.

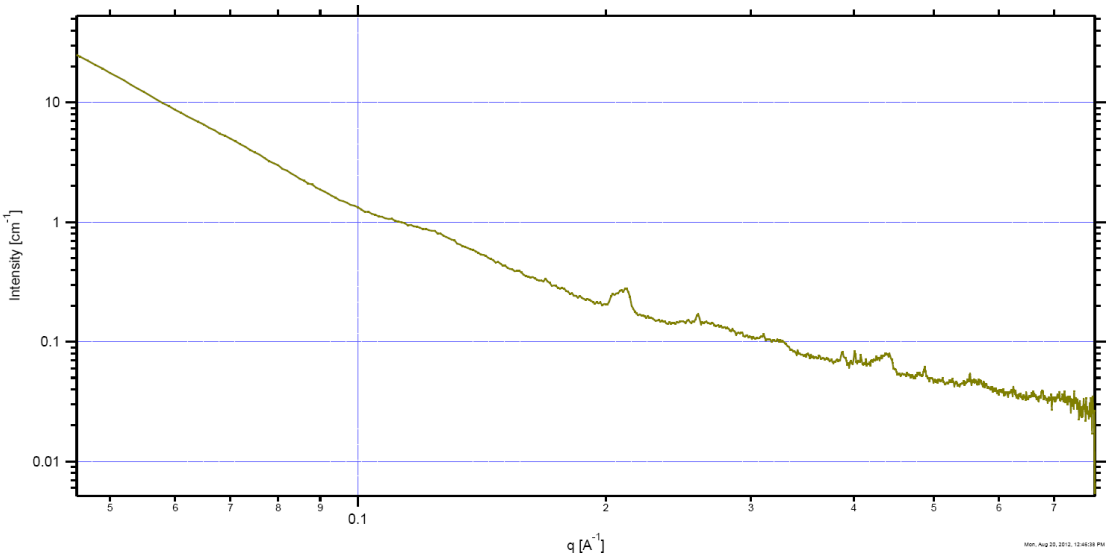

Fig. S6 Small angle X-ray scattering pattern of Ni/MC-750.

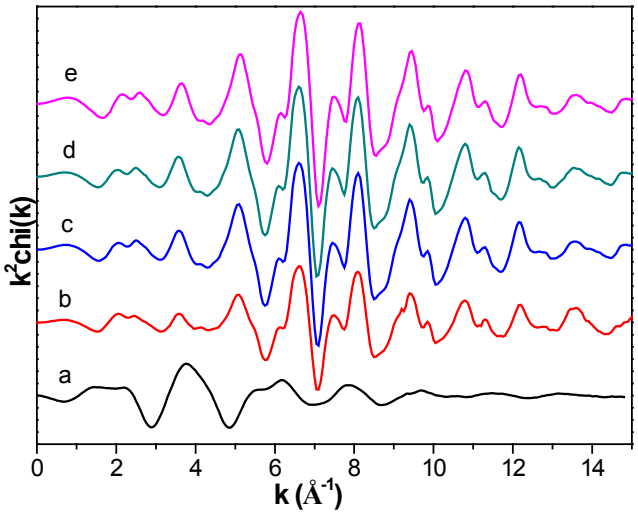

Fig. S7 EXAFS (Ni K-edge scan) plotted as k^2chi(k) *vs.* k for (a) Ni/CTS-P, (b) Ni/MC-550, (c) Ni/MC-750, (d) Ni/MC-950 and (e) Ni foil.

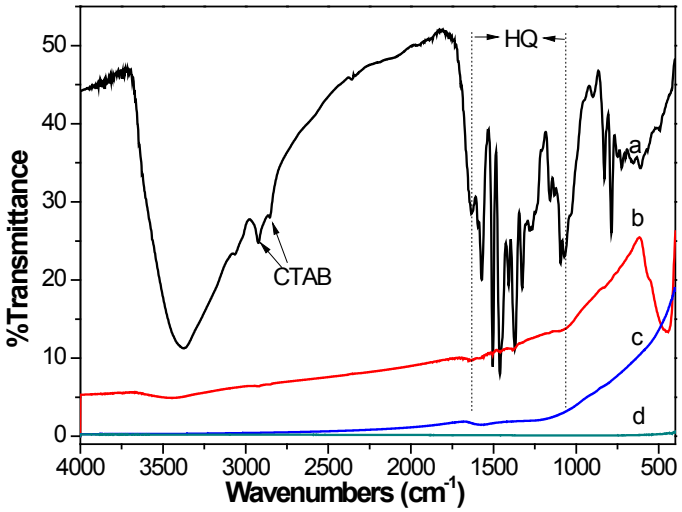

Fig. S8 FT-IR spectra of (a) Ni/CTS-P, (b) Ni/MC-550, (c) Ni/MC-750and (d) Ni/MC-950.

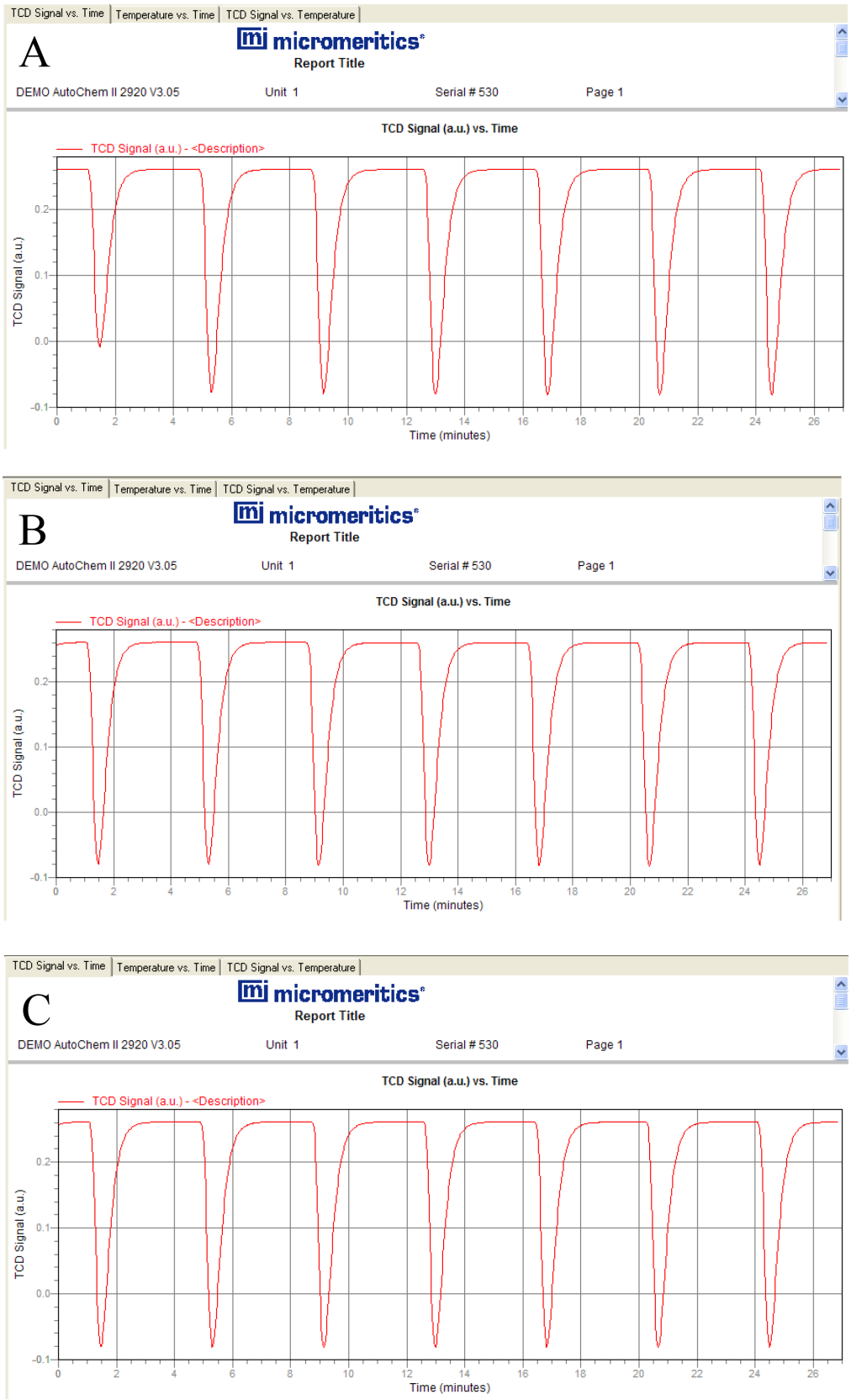

Fig. S9 H_2 chmisorption results for (A) Ni/MC-550, (B) Ni/MC-750 and (C) Ni/MC-950.

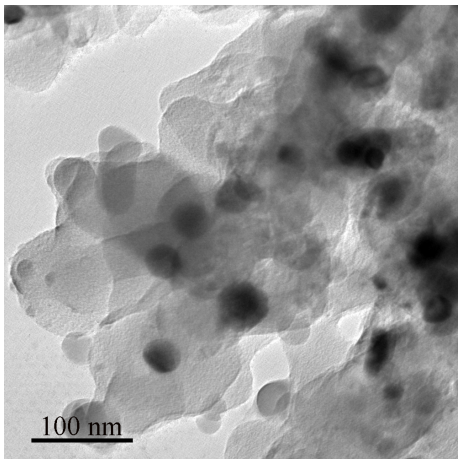

Fig. S10 TEM image of the spent Ni/MC-750.